SCR-623A

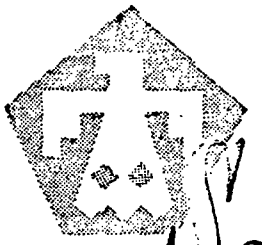

Sandia Corporation

32

REPRINT

TRANSIENT ELECTROMAGNETIC FIELD PROPAGATION THROUGH INFINITE SHEETS, INTO SPHERICAL SHELLS, AND INTO HOLLOW CYLINDERS

by

C W Harrison, Jr

MAY 1964

Transient Electromagnetic Field Propagation Through Infinite Sheets, into Spherical Shells, and into Hollow Cylinders

CHARLES W. HARRISON, JR., SENIOR MEMBER, IEEE

Summary—Gaussian electromagnetic field pulses of several durations are propagated through infinite sheets into the interior of hollow cylinders and into the interior of spherical shells. The plates, spheres and cylinders are made of aluminum and contain no slots. The time history of the propagated pulses is computed. Finally, the time sequence of the electric field is calculated in the interior of a cylinder of finite length when connected at its ends by wires to a generator delivering a current pulse of Gaussian shape.

The dimensions of the cavities are assumed to be sufficiently small so that resonances are not excited by the highest significant frequency contained in the shortest pulse considered. The numerical study is restricted to thin-walled aluminum shields 1/32 inch, 1/16 inch, 1/8 inch and 1/4 inch thick. The half-amplitude widths of the pulses employed lie in the range 14 μsec to 2400 μsec.

It is shown that the resultant Gaussian pulse electric fields defined on the surface of the plates and cylinders are propagated with little diminution in amplitude. This is understandable due to the requirement that the tangential fields are continuous across the interfaces, and to the fact that skin effect is almost nonexistent at low frequencies. The *incident* (as contrasted to *resultant*) field pulse undergoes reflection at the boundary surface. Hence, the attenuation sustained by the *incident* field is great, since *reflection* is the chief mechanism of attenuation of fields at low frequencies. Thin spherical shells form effective magnetic shields. The electric field is small in the interior of thin-walled cylinders carrying extremely large transient currents.

INTRODUCTION

THIS STUDY was undertaken to determine the shielding characteristics of thin-walled infinite sheets, spherical shells and cylindrical tubes, illustrated by Fig. 1, under transient conditions. The shields are made of aluminum and contain no slots. Gaussian electromagnetic field pulses are propagated through the infinite sheets, and from the outside to the inside of closed containers in the geometrical shape of spheres and cylinders. Time histories of the attenuated pulses are computed. For the case of the infinite conductive sheets, the propagated pulses are compared to the associated impinging pulses on the basis of available energy per unit area.

Finally, the field is calculated in the interior of cylindrical tubes of finite length when the ends are connected by wires to a generator delivering a current pulse of Gaussian shape. From the theoretical point of view, this problem is closely related to that of calculating the field within a missile stripped of interior components when subjected to a direct lightning strike.

Manuscript received May 18, 1963; revised September 11, 1963.
The author is a member of the Technical Staff, Sandia Corporation, Sandia Base, Albuquerque, N. M.

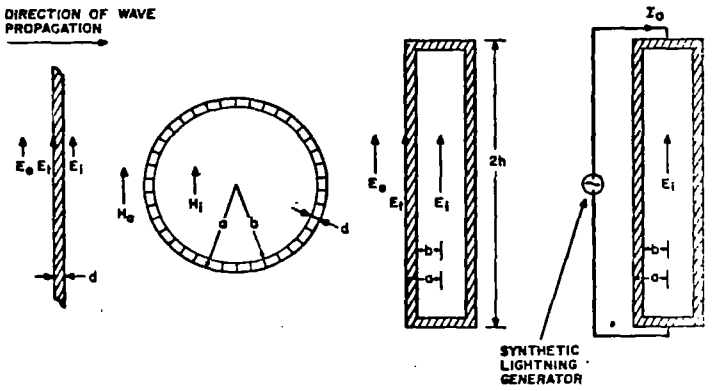

Fig. 1—Configurations considered in the propagation of Gaussian pulses through aluminum walls. (a) Infinite plate. (b) Sphere $\lambda_0 = 2.28b$. (c) Cylinder $\lambda_0 = 2.61b$. (d) Cylinder with direct generator drive, $\lambda_0 = 2.61b$.

THE IMPINGING GAUSSIAN PULSE

The description of the impinging pulse in the time domain employed in this paper is

$$e(t) = Ae^{-(t/t_1)^2/2}, \tag{1}$$

where A is the value of $e(0)$, t is the time, and t_1 is a measure of the pulse width. The spectrum of the pulse is obtained by taking the Fourier transform of (1). Thus,

$$E(f) = A\int_{-\infty}^{\infty} e^{-(t/t_1)^2/2}e^{-j2\pi ft}dt = At_1\sqrt{2\pi}\,e^{-(t/t_1)^2/2}, \tag{2}$$

where

$$f_1 = \frac{1}{2\pi t_1}. \tag{3}$$

In evaluating Fourier transforms by numerical methods, it is necessary to truncate the frequency spectrum in passing from the frequency to time domain, and truncate the limits of integration when computing the frequency spectrum of a given time function.

Let $e_1(t)$ be the new time function obtained by taking the transform of the truncated frequency function. Assume that the cutoff frequency is $f_c = 2.6f_1$. The error is then

$$\eta(t) = |e(t) - e_1(t)| = \left| \int_{-\infty}^{-2.6f_1} E(f)e^{j2\pi ft}df + \int_{2.6f_1}^{\infty} E(f)e^{j2\pi ft}df \right|. \tag{4}$$

Thus

$$\eta(t) \leq 2\int_{2.6f_1}^{\infty} |E(f)|\,df. \tag{5}$$

Substituting (2) into (5) and integrating, $\eta(t) \leq 0.0093A$. Thus $e_1(t)$ does not depart from $e(t)$ by more than 1 per cent at any time.

If $e(t)$ is a plane wave, the energy in the pulse is given by

$$U_t = \frac{1}{\zeta_o}\int_{-\infty}^{\infty}[e(t)]^2dt = \frac{1}{\zeta_o}\int_{-\infty}^{\infty}|E(f)|^2df, \tag{6}$$

where the last relation follows from Parseval's identity. The energy lost by truncation of the spectrum is

$$U_t = \frac{2}{\zeta_o}\int_{2.6f_1}^{\infty}|E(f)|^2df. \tag{7}$$

In these expressions, $\zeta_0 = 120\pi$ ohms is the characteristic resistance of space. Substituting (2) into (6) and (7), and performing the integration, it is found that $U_t = 0.000236U_t$. Thus 0.0236 of 1 per cent of the energy is lost by truncation of the frequency spectrum at $f_c = 2.6f_1$.

In this paper the highest significant frequency contained in a Gaussian pulse is taken to be $f_c = 2.6f_1 = 2.6/2\pi t_1$. The "significant" base width of the time function is $2\times 2.6t_1 = 5.2t_1$. Thus, when $t_1 = 12$ μsec, the pulse duration is considered to be 62.4 μsec. The highest significant frequency in this pulse is 34.48 kc. The half-amplitude width of a Gaussian pulse is $2.355t_1$.

The Transfer Functions for Sheets, Spheres and Cylinders

It is readily shown from elementary principles of electrodynamics that the transfer functions for an infinite metal sheet of thickness d for parallel incidence of the electric field are[1,2]

$$\frac{E_i(f)}{E_o(f)} = \frac{2\zeta_o\zeta}{2\zeta_o\zeta\cos kd + j(\zeta_o^2+\zeta^2)\sin kd} \tag{8}$$

and

$$\frac{E_i(f)}{E_t(f)} = \frac{\zeta_o}{\zeta_o\cos kd + j\zeta\sin kd}, \tag{9}$$

where $E_i(f)$ is the electric field emerging from the far side of the sheet, $E_o(f)$ is the incident electric field and $E_t(f)$ is the tangential electric field on the near side of the sheet.[3] Thus $E_t(f)$ is the vector sum of the incident and reflected fields. $E_o(f) \gg E_i(f)$, and when $f > o$, $E_t(f) > E_i(f)$ because of skin effect. (See Fig. 1.)

$$\zeta = \sqrt{\frac{\pi f\mu}{\sigma}}(1+j), \tag{10}$$

$$k = \sqrt{\pi f\mu\sigma}\,(1-j) \tag{11}$$

where $\mu = 4\pi\times 10^{-7}$ h/m is the permeability of space and $\sigma = 3.72\times 10^7$ mho/m is the conductivity of aluminum. In deriving (8) and (9), a time dependence of the form $\exp(j2\pi ft)$ is assumed.

The transfer function for a spherical shell is[4]

$$\frac{H_i(f)}{H_o(f)} = \frac{3(\gamma a)^{1/2}}{(\gamma b)^{5/2}[I_{-1/2}(\gamma a)K_{-5/2}(\gamma b) - K_{-1/2}(\gamma a)I_{-5/2}(\gamma b)]}. \tag{12}$$

Here, H_i is the magnetic field inside the spherical shell at its center, H_o is the resultant magnetic field at a great distance from the sphere, a is the outer radius of the shell, b is the inner radius of the shell and $d = a - b$ is the shell thickness.

$$\gamma = \sqrt{\pi f\mu\sigma}\,(1+j). \tag{13}$$

I and K are the modified Bessel functions of the first and second kind.

Using the exact relations,[5]

$$\left.\begin{aligned} I_{-1/2}(x) &= \sqrt{\frac{2}{\pi x}}\cosh x \\ I_{-5/2}(x) &= \sqrt{\frac{2}{\pi x}}\left(\cosh x - \frac{3}{x}\sinh x + \frac{3}{x^2}\cosh x\right) \\ K_{-1/2}(x) &= \sqrt{\frac{\pi}{2x}}e^{-x} \\ K_{-5/2}(x) &= \sqrt{\frac{\pi}{2x}}e^{-x}\left(1+\frac{3}{x}+\frac{3}{x^2}\right) \end{aligned}\right\}. \tag{14}$$

[1] J. A. Stratton, "Electromagnetic Theory," McGraw-Hill Book Co., Inc., New York, N. Y., ch. 9, sec. 9.10, pp. 511–513; 1941.

[2] L. E. Kinsler and A. R. Frey, "Fundamentals of Acoustics," John Wiley and Sons, Inc., New York, N. Y., ch. 6, sec. 6.4, pp. 149–154; 1950.

[3] The subscripts *i*, *o*, and *t* on the fields mean *inside*, *outside* and *tangential* (or *total*), respectively.

[4] L. V. King, "Electromagnetic shielding at radio frequencies," *Phil. Mag. J. Sci.*, vol. 15, no. 97, pp. 201–223; February, 1933. There appear to be a number of inconsistencies in this paper. If the time dependence is taken to be $\exp(j2\pi ft)$, King's formula (16) reproduced in this paper as (12) appears to be correct, provided $\kappa = \gamma = \sqrt{\pi f\mu\sigma}(1+j)$. Note that (12) is the quasi-static solution of the spherical shield problem.

[5] N. W. McLachlan, *Bessel Functions for Engineers*, 2nd ed., Oxford University Press, New York, N. Y., (*list of formulas*), pp. 190–214; 1955.

Eq. (12) can be reduced to the following identity which is more convenient for computation:

$$\frac{H_i(f)}{H_o(f)} = \frac{3\gamma a}{(\gamma b)^2\left[\left(1+\frac{3}{(\gamma b)^2}\right)\sinh \gamma d + \frac{3}{\gamma b}\cosh \gamma d\right]}. \quad (15)$$

The cylinder transfer functions are[6]

$$\frac{E_i(f)}{E_t(f)} = \frac{J_o(kb)N_1(kb) - N_o(kb)J_1(kb)}{J_o(ka)N_1(kb) - N_o(ka)J_1(kb)} \quad (16)$$

and

$$\frac{E_t(f)}{I_o(f)} = \frac{1}{\pi\sigma a^2}\left(\frac{ka}{2}\right)\cot kd. \quad (17)$$

In deriving (16) and (17), a time dependence of the form $\exp(j2\pi ft)$ is assumed. Here a and b are the outer and inner radii of the tube, respectively, and $d=a-b$ is the wall thickness.

Now[7]

$$J_o(kb)N_1(kb) - N_o(kb)J_1(kb) = -\frac{2}{\pi kb}. \quad (18)$$

(This is the Wronskian relation.) Combining (16) and (17) and making use of (18),

$$\frac{E_i(f)}{I_o(f)} = -\frac{\cot kd}{\pi^2\sigma ab}\left[\frac{1}{J_o(ka)N_1(kb) - N_o(ka)J_1(kb)}\right]. \quad (19)$$

This expression permits calculation of the steady-state field within the cylinder in terms of the total current delivered by the current generator directly connected by wires to the ends of the cylinder. It is assumed that the current is uniform in this circuit. This will be the case if the circuit dimensions are small in terms of the wavelength of the highest significant frequency contained in the shortest current pulse employed in this study.

If a plane-wave electric field is directed parallel to the axis of an isolated cylinder, the current $I_o(f)$ at its midpoint is obtained from antenna theory. It is given by the relation

$$I_o(f) = \frac{2h_e(f)E_o(f)}{Z_o(f)}. \quad (20)$$

The effective length of the cylinder is $2h_e$, and Z_o is its impedance. If $\Omega \geq 7$ and $\beta h = (2\pi/\lambda)h \leq (2\pi f_c/c)h \leq 0.5$,[8]

$$2h_e(f) = \frac{h(\Omega-1)}{\Omega - 2 + \ln 4} \quad (21)$$

and

$$Z_{of} = -j\frac{\zeta_o(\Omega - 2 - 2\ln 2)}{2\pi\beta h}\cdot\left[1 + j\frac{(\beta h)^3}{3(\Omega - 2 - 2\ln 2)}\right], \quad (22)$$

where Ω is the cylinder shape parameter. It is

$$\Omega = 2\ln\frac{2h}{a}. \quad (23)$$

The length of the cylinder is $2h$.

It is of interest to note that as $f \to o$, the transfer functions (8), (9), (15), (16) and (17) become

$$\left.\frac{E_i(o)}{E_o(o)}\right|_{\text{plate}} = \frac{1}{1+\frac{\zeta_o\sigma d}{2}} \quad (24a)$$

$$\left.\frac{E_i(o)}{E_t(o)}\right|_{\text{plate}} = 1 \quad (24b)$$

$$\left.\frac{H_i(o)}{H_o(o)}\right|_{\text{sphere}} = 1 \quad (24c)$$

$$\left.\frac{E_i(o)}{E_t(o)}\right|_{\text{cylinder}} = 1 \quad (24d)$$

$$\left.\frac{E_t(o)}{I_o(o)}\right|_{\text{cylinder}} = \frac{1}{2\pi\sigma ad}. \quad (24e)$$

Also, from (20), as $f \to o$,

$$I_o(o)\,|_{\text{antenna}} = 0. \quad (24f)$$

It is deemed appropriate to physically justify results (24a) and (24b). Several of the other results in (24) may be inferred from this discussion. The fact that $E_i(o)/E_o(o)$ does not reduce to unity as $f \to o$ is understandable on the basis of the wave impedance concept and the transmission line analogy of wave propagation.[9] Shielding is due to two effects; one of these is skin effect and the other is reflection that takes place at the outer surface of the shield. The more important mechanism at low frequencies is the one of reflection. The incident field E_o is in large measure reflected by the plate. The fact

[6] C. W. Harrison, Jr. and R. W. P. King, "Response of a loaded electric dipole in an imperfectly conducting cylinder of finite length," *J. Res. NBS—D. Radio Propagation*, vol. 64D, no. 3, see Eqs. (15) and (26) on pp. 290–291; June, 1960.

[7] McLachlan, *op. cit.*, see p. 32.

[8] R. W. P. King, "Theory of Linear Antennas," Harvard University Press, Cambridge, Mass., ch. 2, sec. 31, eq. (6), p. 184, and ch. 4, sec. 9, eq. (21), p. 487; 1956.

[9] S. Ramo and J. R. Whinnery, "Fields and Waves in Modern Radio," John Wiley and Sons, Inc., New York, N. Y., 2nd ed., pp. 286–314; 1953.

that $E_i(o)/E_t(o)$ reduces to unity as $f \to o$ is just another way of saying that the resultant tangential fields must be continuous across the interfaces, and at low frequencies skin effect is almost nonexistent. Hence, the resultant or total field on the near side of the plate must equal the resultant field emerging from the far side. It should be mentioned that E_t is also a good approximation to the resultant field in the vicinity of the near side of the plate when the wavelength is long.

Let

$$G(f) = G_R(f) + jG_I(f) \tag{25}$$

represent any one of the foregoing transfer functions. It can be readily verified by expanding the trigonometric, hyperbolic and Bessel functions in series, and by examining the resulting expressions that they satisfy the relation

$$G^*(f) = G(-f). \tag{26}$$

That this holds for (20) follows from the fact that $Z_o^*(f) = Z_o(-f)$, as an inspection of (22) shows. Eq. (26) sets forth an important property of any transfer function applying to a physically realizable system.

From (25)

$$G(-f) = G_R(-f) + jG_I(-f), \tag{27}$$

and by definition

$$G^*(f) = G_R(f) - jG_I(f). \tag{28}$$

It follows that

$$G_R(f) = G_R(-f) \tag{29}$$

is an even function, and

$$G_I(f) = -G_I(-f) \tag{30}$$

is an odd function.

The Form of the Integrals to be Evaluated by a Computer

For illustrative purposes, let it be supposed that the time function of the electric field within a hollow cylinder is to be computed in terms of the Gaussian pulse current which the generator delivers by wire to the ends of the cylinder. In this instance, $G(f)$ is the shorthand notation for the right-hand side of (19). Then

$$E_i(f) = G(f)I_o(f). \tag{31}$$

$I_o(f)$ corresponds to (2), *i.e.*,

$$I_o(f) = At_1\sqrt{2\pi}\, e^{-(f/f_1)^2/2} \tag{32}$$

for a current pulse in the time domain corresponding to (1). A is in amperes, and $I_o(f)$ in a/Hz for this particular situation.

The time history of the field on the interior of the cylinder is available from the integral

$$e_i(t) = At_1\sqrt{2\pi}\int_{-\infty}^{\infty} G(f)e^{-(f/f_1)^2/2}e^{j2\pi ft}df$$

$$\sim At_1\sqrt{2\pi}\int_{-f_c}^{f_c}\{G_R(f)\cos 2\pi ft - G_I(f)\sin 2\pi ft + j[G_R(f)\sin 2\pi ft + G_I(f)\cos 2\pi ft]\}$$

$$\cdot e^{-(f/f_1)^2/2}df, \tag{33}$$

provided the time dependence assumed in deriving $G(f)$ is exp $(j2\pi ft)$. Since $G_R(f)$ and cos $2\pi ft$ are even functions, and $G_I(f)$ and sin $2\pi ft$ are odd functions, it follows that (33) reduces to

$$e_i(t) = 2At_1\sqrt{2\pi}\int_0^{f_c}[G_R(f)\cos 2\pi ft - G_I(f)\sin 2\pi ft]\cdot e^{-(f/f_1)^2/2}df. \tag{34}$$

This is the final form of the integral to be evaluated on the computer. Note that the integral is necessarily real because $e_i(t)$ is a real function of time. All of the integrals encountered in this paper concerning the various shields are similar in form to (34). The constant A was taken as unity throughout the work. Of course, the units of A will depend on the shielding problem being considered.

Discussion of Graphs

Graph 1 shows the amplitude-time relation of some of the input Gaussian pulses used in the numerical study. Specifically, pulses are drawn for values t_1 of 6, 12, 24, and 48 μsec. Note that the peak amplitude of unity occurs at zero time. The pulses are symmetrical on the time scale.

Graph 2, based on (9), gives the steady-state transfer characteristic relating $E_i(f)$ to $E_t(f)$ for an infinite aluminum plate of thickness 1/32 inch, 1/16 inch, and 1/8 inch. For example, for a 1/8-inch plate at 120 kc, the field emerging from the plate $E_i(f)$ is 110 db below the tangential field $E_t(f)$ (or the resultant field) on the other side of the plate.

Graphs 3, 4, 5, and 6 give the time history of the field $e_i(t)$ emerging from the plates of designated thicknesses in terms of $e_t(t)$ for values of t_1 of 6, 12, 24, and 48 μsec, respectively. The value of $e_t(o)$ is 1 vpm. Note that, in all cases, the attenuation of the field is not great, but progressively increases with plate thickness and decreasing values of t_1. The waves are retarded in

time in propagating through the plates, as should be anticipated. The delay increases with plate thickness.

Graph 7, based on (8), is like Graph 2, except that $e_o(t)$ replaces $e_i(t)$.

Graphs 8, 9, 10, and 11 correspond to Graphs 3, 4, 5, and 6, respectively, except that $e_o(t)$ replaces $e_i(t)$. Note that the wave shapes are very much alike, but the amplitude scale is vastly different. Graph 8 shows, for example, that when the peak value of $e_o(t)$ is 1 vpm, $t_1 = 6$ μsec and $d = 1/32$ inch, the peak value of $e_i(t)$ is about 1.61×10^{-7} vpm, and occurs at about 0.005 msec. If $e_0(o) = 10^5$ vpm, $e_i(t) = 0.0161$ vpm. Note that $e_0(t)$ undergoes reflection at the boundary surface, and this accounts for the large attenuation afforded by the sheet.

Graph 12, based on (15), gives the steady-state transfer characteristic relating $H_i(f)$ to $H_o(f)$ for a 36-inch spherical shell made of aluminum having wall thicknesses of 1/32 inch, 1/16 inch and 1/8 inch. As an illustration, for a 1/16-inch wall 36-inch sphere at 7 kcs, the magnetic field $H_i(f)$ on the interior of the sphere is 56 db below the magnetic field $H_o(f)$ outside.

Graphs 13, 14, 15, and 16 give the time history of the magnetic field $h_i(t)$ inside the 36-inch spheres of designated wall thicknesses when the magnetic field $h_o(o) = 1$ ampere/m for t_1 values of 24, 48, 96, and 1000 μsec, respectively. As expected, as the pulse length increases, the field $h_i(t)$ increases. The thicker the shield, the more effective it becomes. Note the severe distortion of the resultant pulse in propagating into the interior of the sphere.

Graph 17 is like Graph 12, except that it applies to a 72-inch spherical shell.

Graphs 18, 19, 20, and 21 correspond to Graphs 13, 14, 15, and 16, respectively, except that the computations were carried out for a 72-inch spherical shell.

Graph 22, based on (16), gives the steady-state transfer characteristic relating $E_i(f)$ to $E_i(f)$ for a cylinder 22.08 feet in length and 16 inches in diameter when the wall thicknesses are 1/32 inch, 1/16 inch and 1/8 inch.

Graphs 23, 24, and 25 give the time history of the field $e_i(t)$ in the interior of the above cylinder when $e_i(o) = 1$ vpm for t_1 values of 6, 12, and 24 μsec. These graphs applying to infinite cylinders have much in common with Graphs 3, 4, and 5 applying to infinite plates.

Graph 26, computed from (16), (17), and (20), permits one to obtain the db ratio of $E_i(f)$ to $E_o(f)$ under steady-state conditions for a cylinder 22.08 feet in length and 16 inches in diameter, when the plate thickness and frequency are specified. The transfer characteristic $E_i(f)$ to $E_o(f)$ is obtained by eliminating $I_o(f)$ between (19) and (20).

Graphs 27, 28, and 29 furnish the time history of $e_i(t)$ for $e_o(o)$ of 1 vpm for the designated cylinder for t_1 values of 6, 12, and 24 μsec and for wall thicknesses of 1/32 inch, 1/16 inch and 1/8 inch. Note that the interior field is extremely minute in terms of the incident field. Most of this attenuation is due to the fact that the incident field is reflected by the cylinder; the field $e_i(t)$ is extremely small compared to $e_o(t)$. In the computation associated with these graphs, the real part of the transfer function is very small and the imaginary part rises almost linearly with increasing frequency over the range of integration of (34). Consequently, the output signal is approximately the time derivative of the input signal, as the curves show. The phenomenon is not to be attributed to antenna resonance. The cylinder remains short in terms of the wavelength of the highest significant frequency contained in the shortest pulse considered in the analysis.

Graph 30, computed from (19), furnishes the ratio of $E_i(f)/I_o(f)$ as a function of frequency for a cylinder 22.08 feet in length and 16 inches in diameter having wall thicknesses of 1/32 inch, 1/16 inch and 1/8 inch. Thus, for a total current in any cross section of the cylinder of 1 ampere, the field in the interior of the cylinder will be 10^{-10} vpm, if the frequency is 150 kc and the cylinder wall thickness is 1/8 inch.

Graphs 31, 32, and 33 give the time history of $e_i(t)$ when $i_o(o)$ is 1 ampere, for the cylinders mentioned above for t_1 values of 12, 24, and 48 μsec.

Graph 34 is the same as Graph 30, but is computed for a cylinder 105 inches in diameter, 60 feet and 4 inches in height, and having a wall thickness of 1/4 inch. These dimensions are reported to apply to a Jupiter missile.

Graph 35 presents the time history of the electric field $e_i(t)$ inside a Jupiter missile stripped of interior components when $i_o(o)$ is 1 ampere for t_1 values of 24, 48 and 96 μsec. Observe that the height dimension of the missile is sufficiently small so that the current is uniform in the circuit connecting the ends of the missile to the current pulse generator.

Table I presents the decibel ratio of the energy available in the emerging plane-wave pulse from the far side of the plate to the energy in the impinging plane-wave pulse on the near side of the plate for the cases of tangential and incident electric fields. The decibel ratio of the propagated and impinging pulse peaks in the various situations described in the paper is easily obtained by inspection, hence tables are not provided.

Table I was computed from the relation

$$\text{db} = 10 \log_{10} \left\{ \frac{\int_{-\infty}^{\infty} [e_i(t)]^2 dt}{\int_{-\infty}^{\infty} [e_{(i)}(t)]^2 dt} \right\}$$

$$= 10 \log_{10} \left\{ \frac{\int_{-\infty}^{\infty} [e_i(t)]^2 dt}{t_1 \sqrt{\pi}} \right\}. \qquad (35)$$

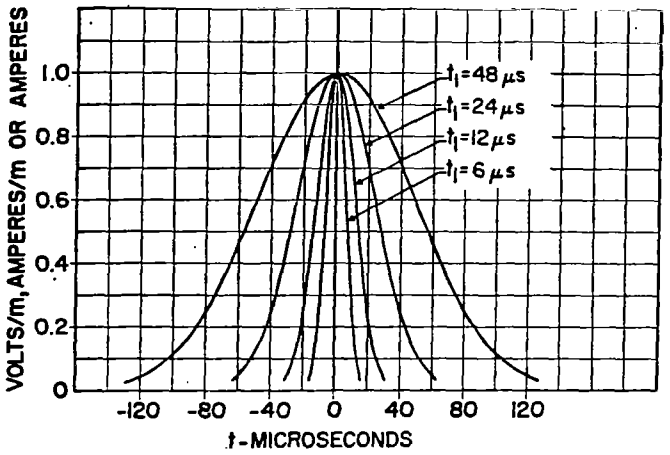

Graph 1—Input Gaussian pulses.

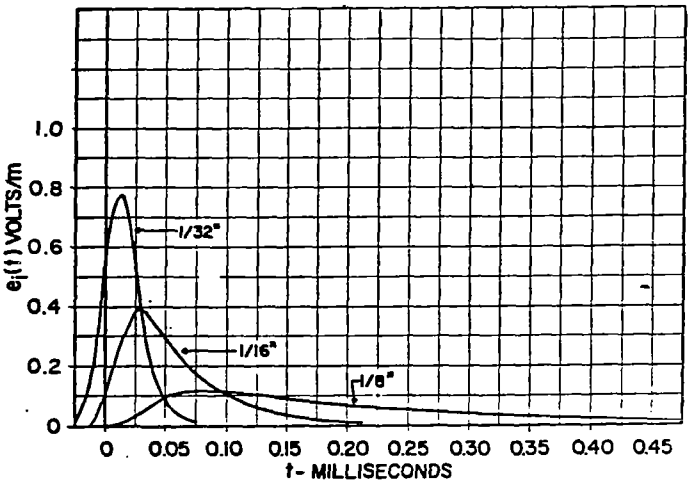

Graph 4—Infinite plate. $e_i(o) = 1$ vpm; $t_1 = 12$ μsec.

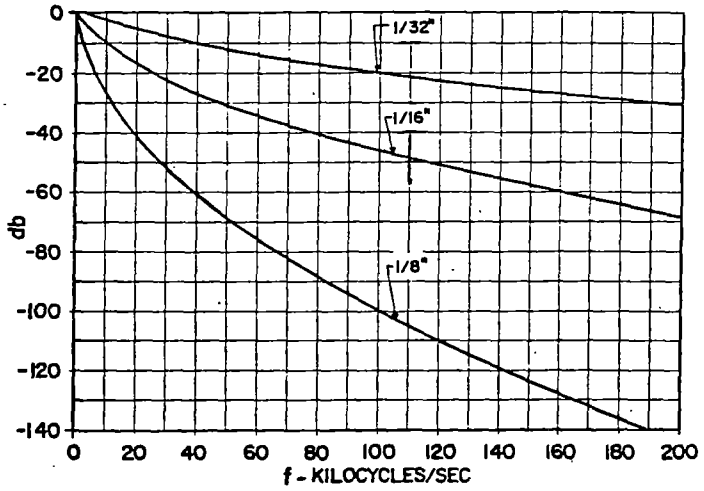

Graph 2—Infinite plate. Steady-state transfer characteristic relating $E_i(f)$ to $E_i(f)$.

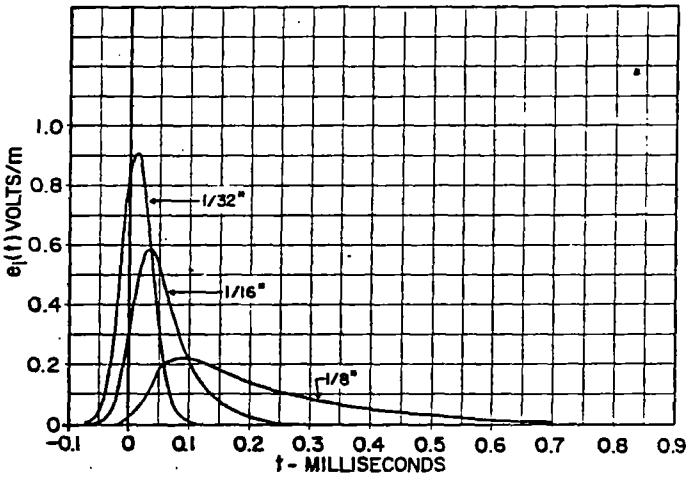

Graph 5—Infinite plate. $e_i(o) = 1$ vpm; $t_1 = 24$ μsec.

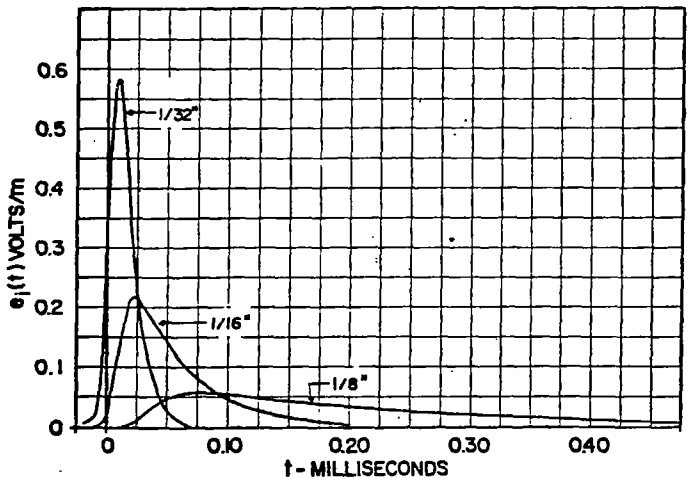

Graph 3—Infinite plate. $e_i(o) = 1$ vpm; $t_1 = 6$ μsec.

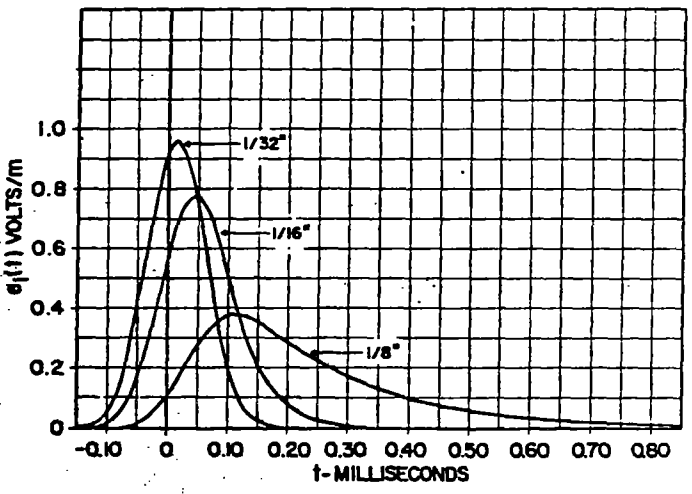

Graph 6—Infinite plate. $e_i(o) = 1$ vpm; $t_1 = 48$ μsec.

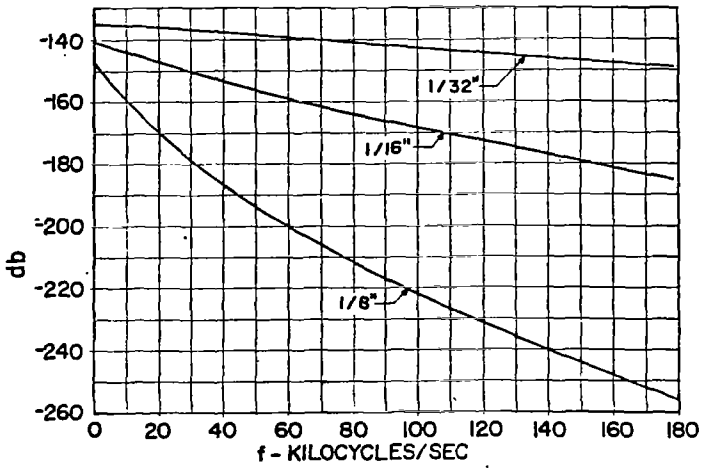

Graph 7—Infinite plate. Steady-state transfer characteristic relating $E_i(f)$ to $E_o(f)$.

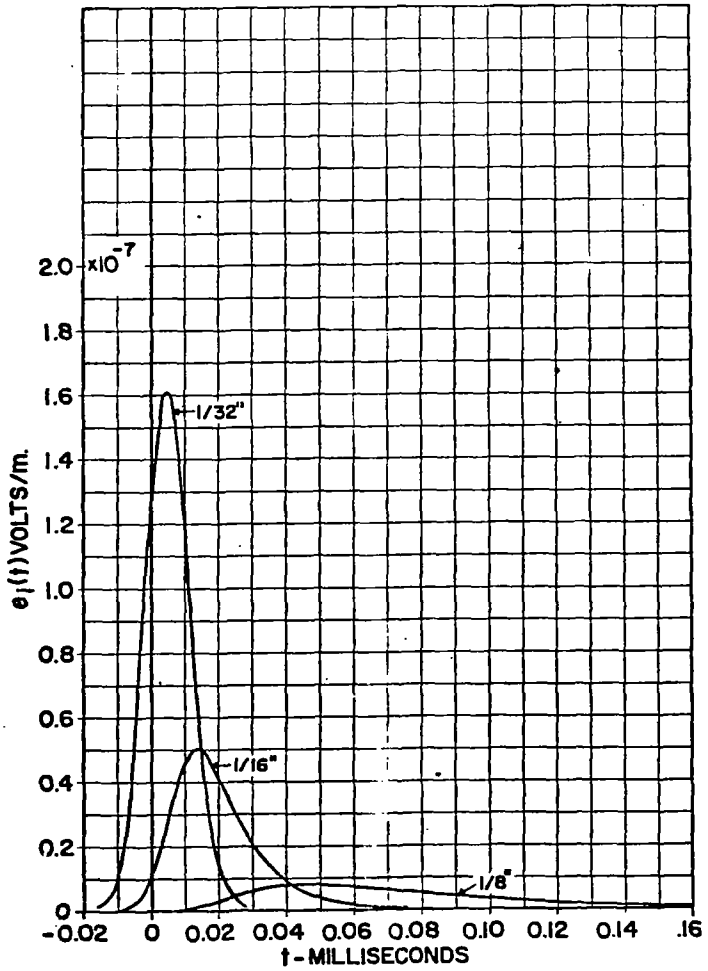

Graph 8—Infinite plate. $e_o(o) = 1$ vpm; $t_1 = 6$ μsec.

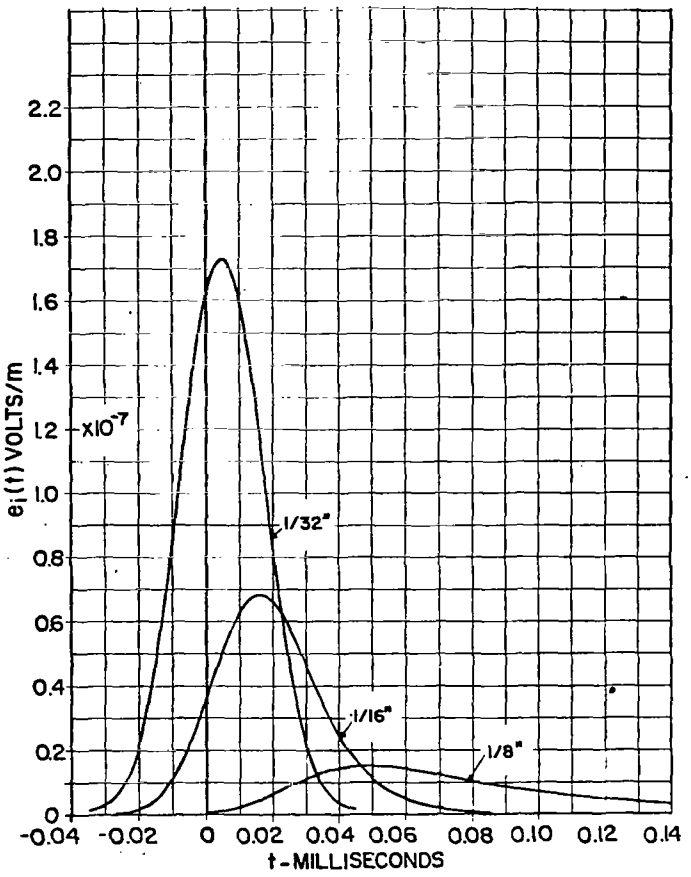

Graph 9—Infinite plate. $e_o(o) = 1$ vpm; $t_1 = 12$ μsec.

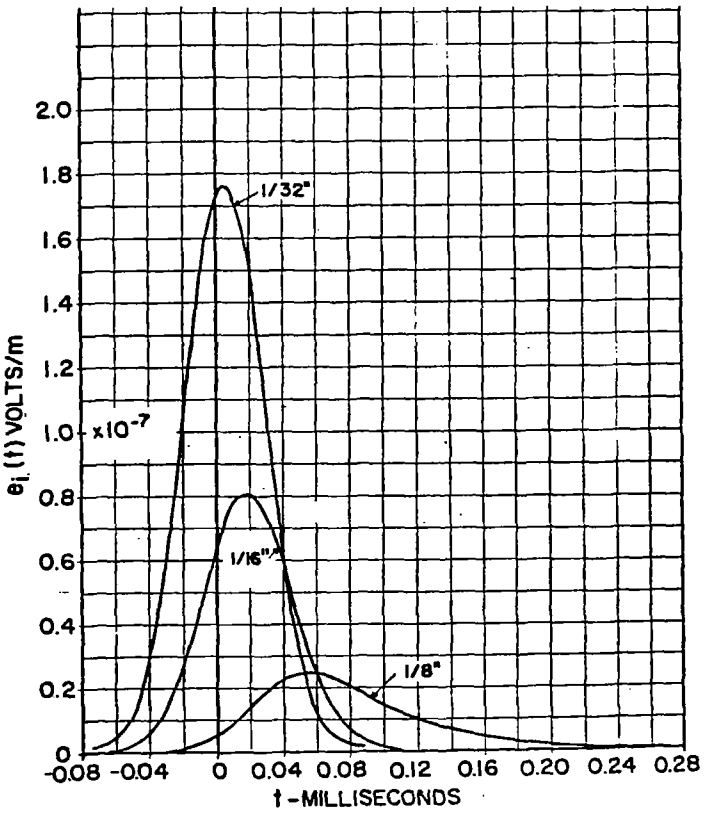

Graph 10—Infinite plate. $e_o(o) = 1$ vpm; $t_1 = 24$ μsec.

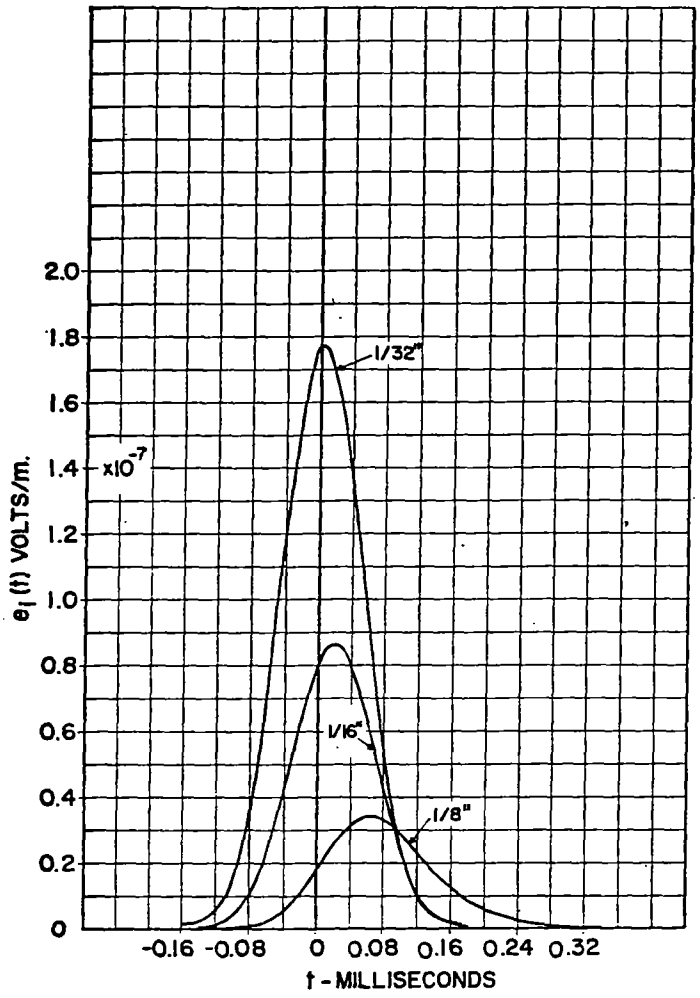

Graph 11—Infinite plate. $e_s(o)=1$ vpm; $t_1=48$ μsec.

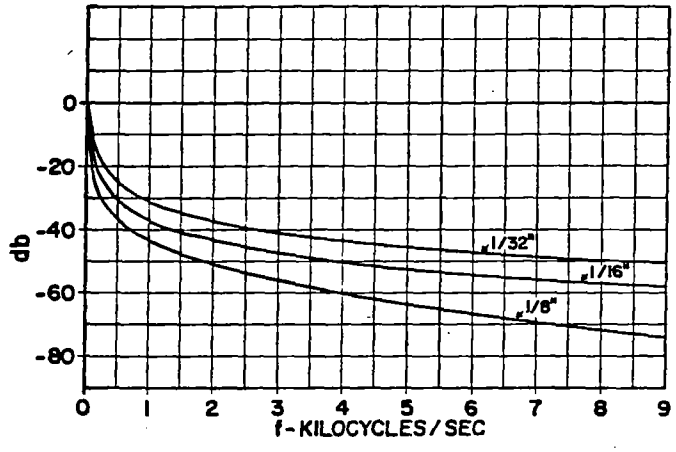

Graph 12—Sphere 36 inches in diameter. Steady-state transfer characteristic relating $H_i(f)$ to $H_s(f)$.

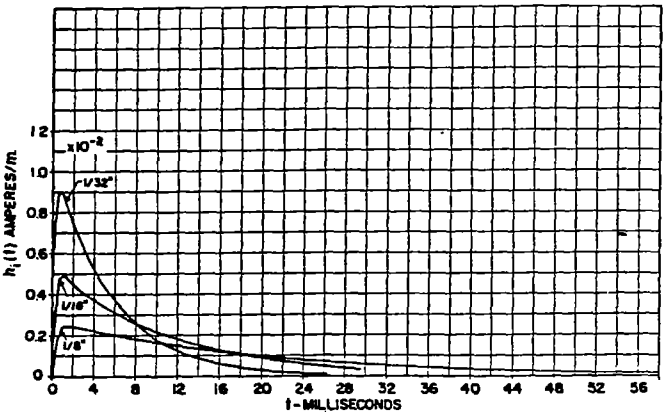

Graph 13—Sphere 36 inches in diameter. $h_s(o)$ = 1 ampere/m; $t_1=24$ μsec.

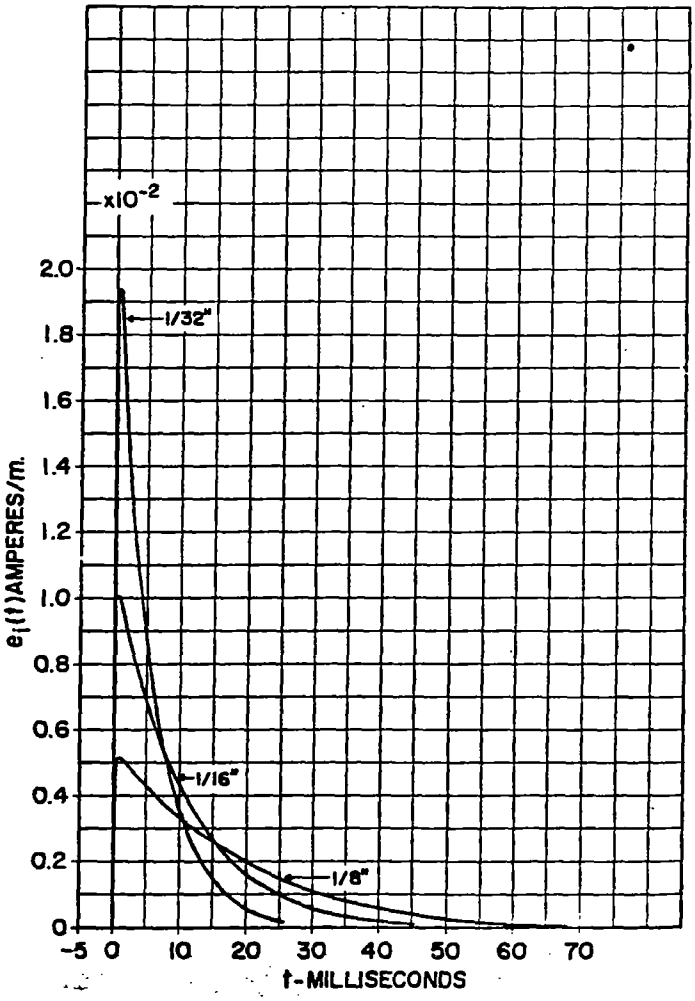

Graph 14—Sphere 36 inches in diameter. $h_s(o)$ = 1 ampere/m; $t_1=48$ μsec.

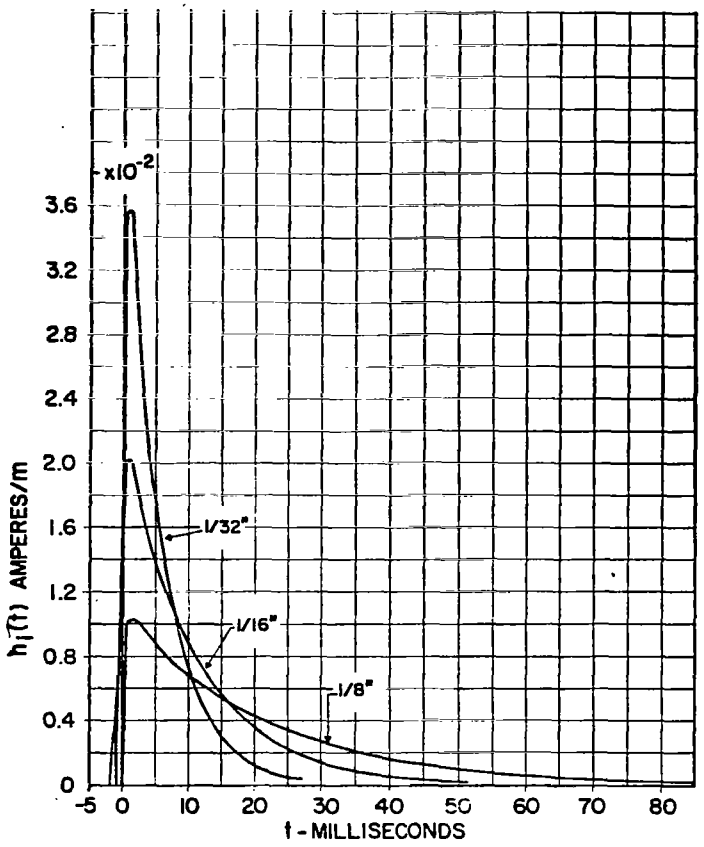

Graph 15—Sphere 36 inches in diameter. $h_o(o)$ = 1 ampere/m; t_1 = 96 μsec.

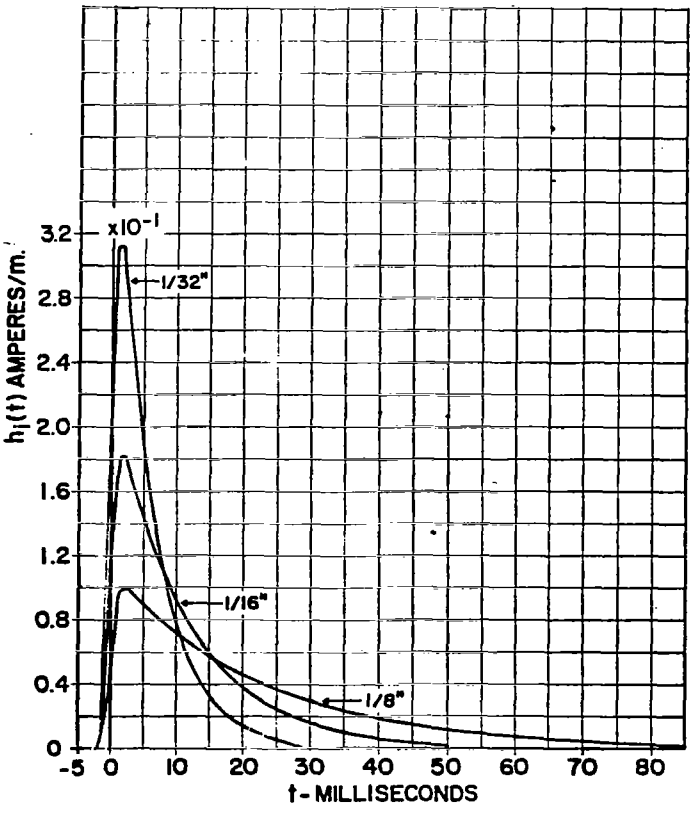

Graph 16—Sphere 36 inches in diameter. $h_o(o)$ = 1 ampere/m; t_1 = 1000 μsec.

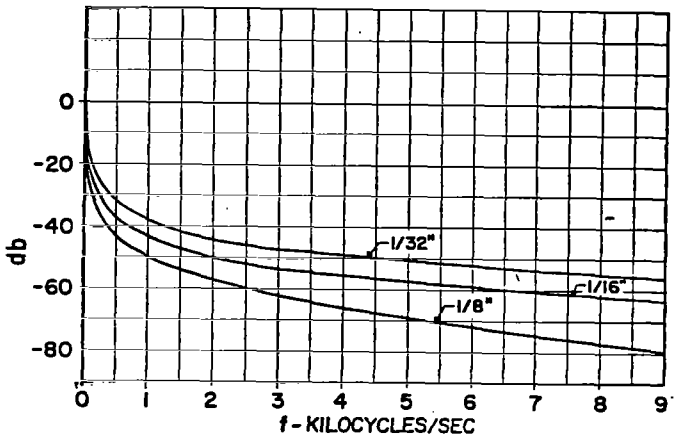

Graph 17—Sphere 72 inches in diameter. Steady-state transfer characteristic relating $H_i(f)$ to $H_o(f)$.

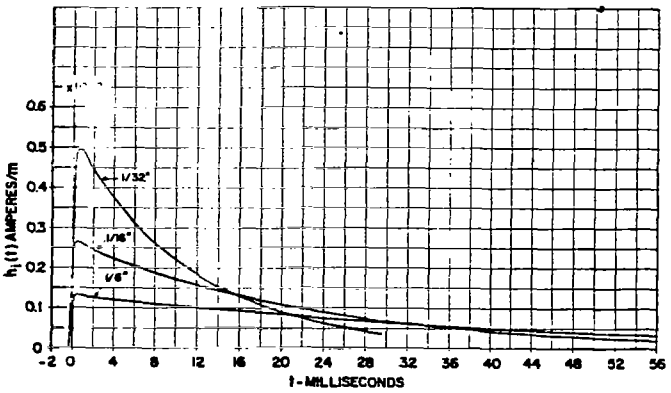

Graph 18—Sphere 72 inches in diameter. $h_o(o)$ = 1 ampere/m; t_1 = 24 μsec.

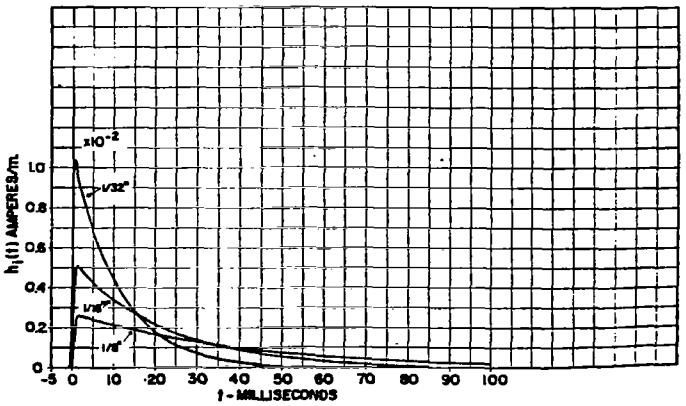

Graph 19—Sphere 72 inches in diameter. $h_o(o)$ = 1 ampere/m; t_1 = 48 μsec.

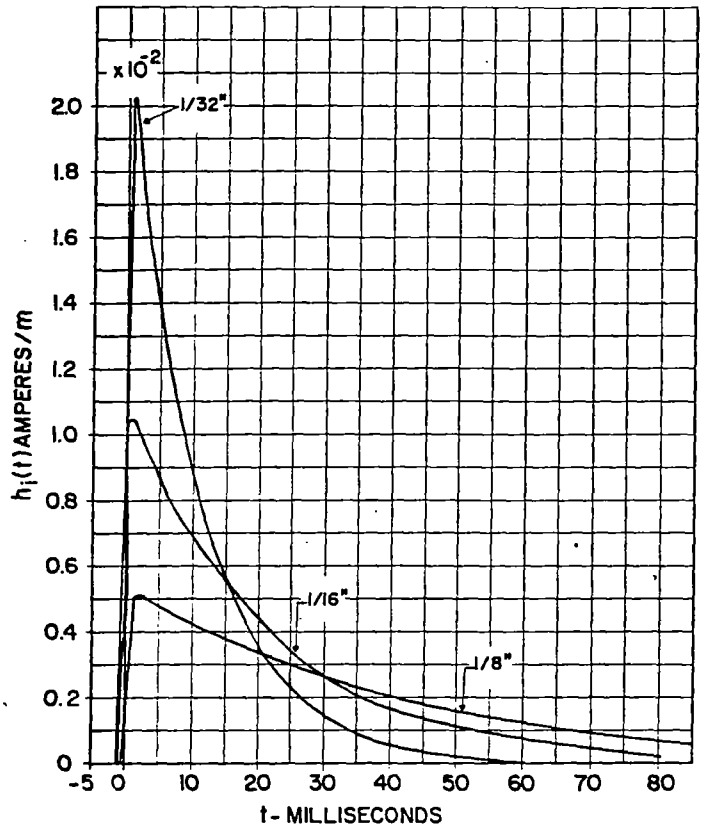

Graph 20—Sphere 72 inches in diameter. $h_s(o)$ = 1 ampere/m; t_1 = 96 μsec.

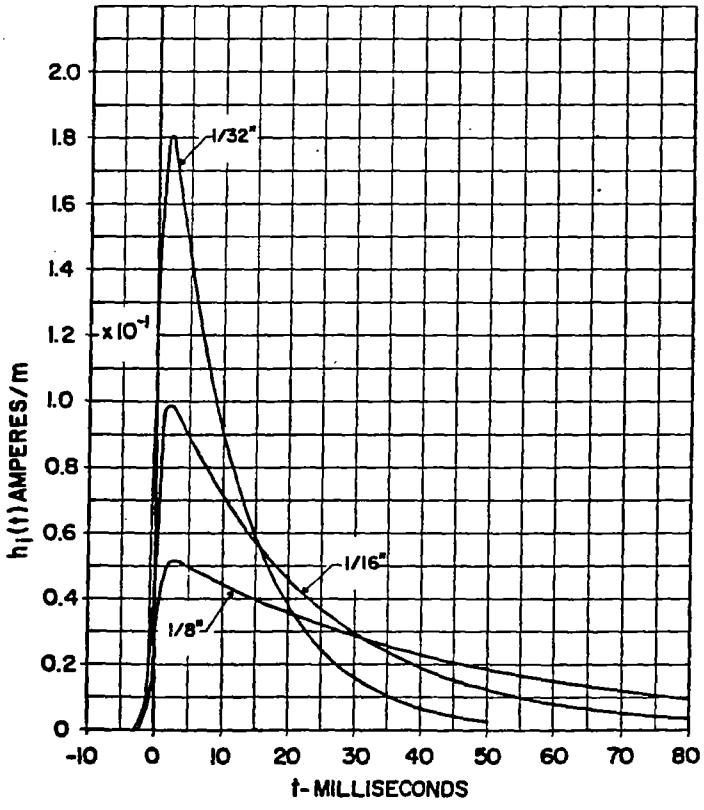

Graph 21—Sphere 72 inches in diameter. $h_s(o)$ = 1 ampere/m; t_1 = 1000 μsec.

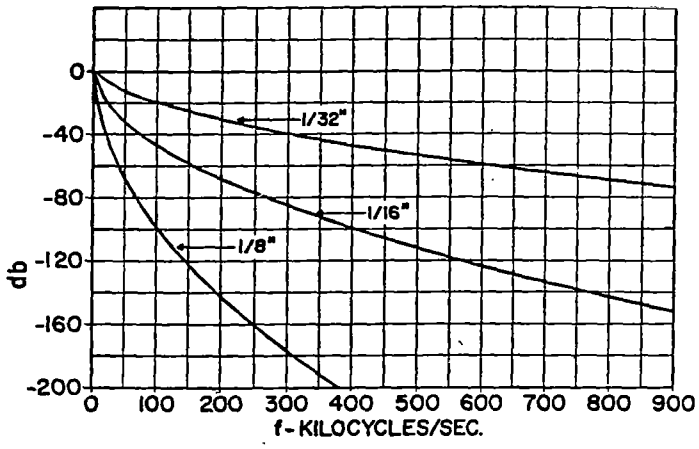

Graph 22—Cylinder. Steady-state transfer characteristic relating $E_s(f)$ to $E_i(f)$.

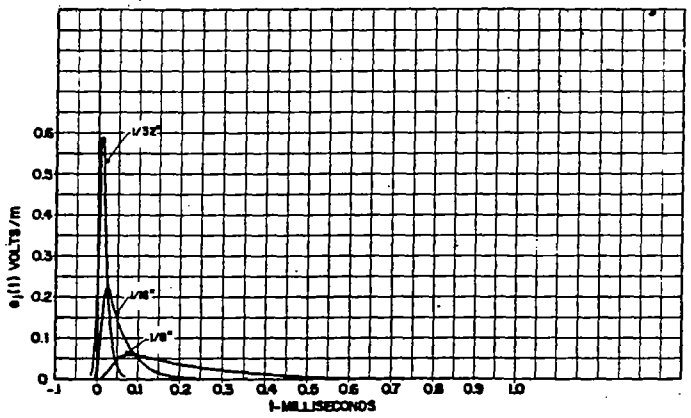

Graph 23—Cylinder. $e_i(o)$ = 1 vpm; t_1 = 6 μsec.

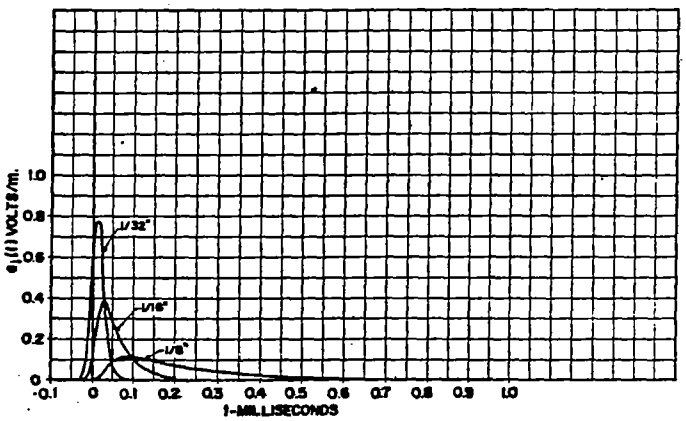

Graph 24—Cylinder. $e_i(o)$ = 1 vpm; t_1 = 12 μsec.

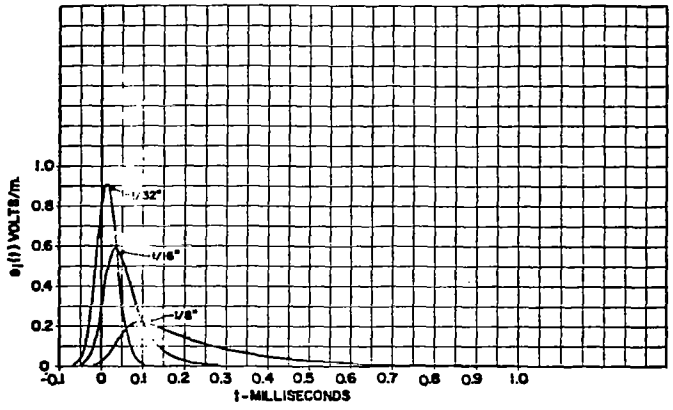

Graph 25—Cylinder. $e_i(o)=1$ vpm; $t_1=24$ μsec.

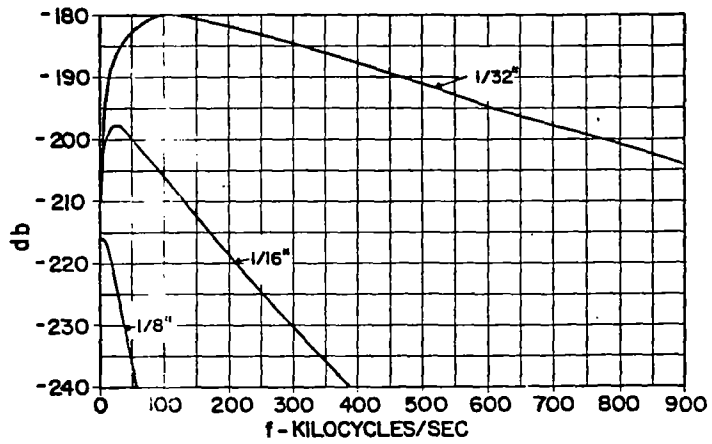

Graph 26—Cylinder. Steady-state transfer characteristic relating $E_i(f)$ to $E_o(f)$.

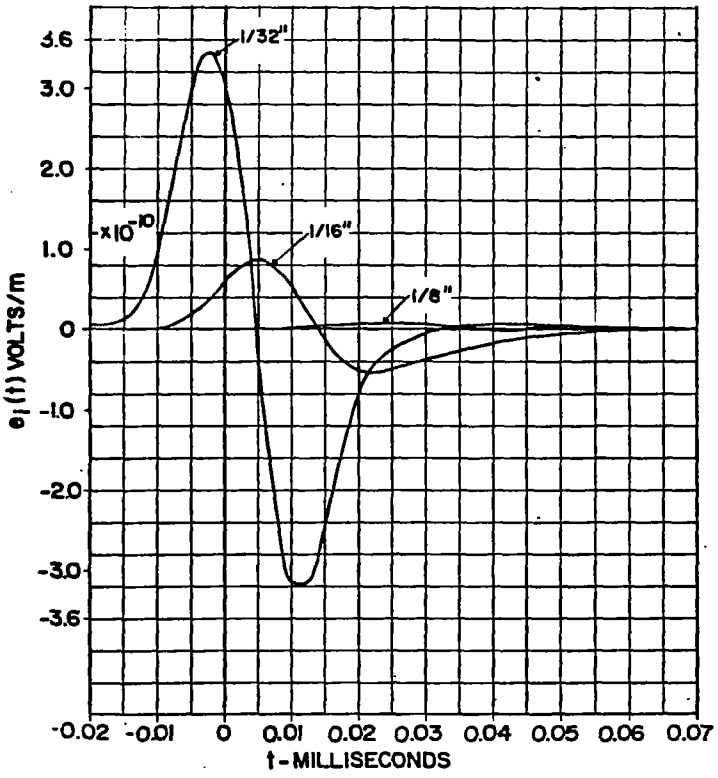

Graph 27—Cylinder. $e_o(o)=1$ vpm; $t_1=6$ μsec.

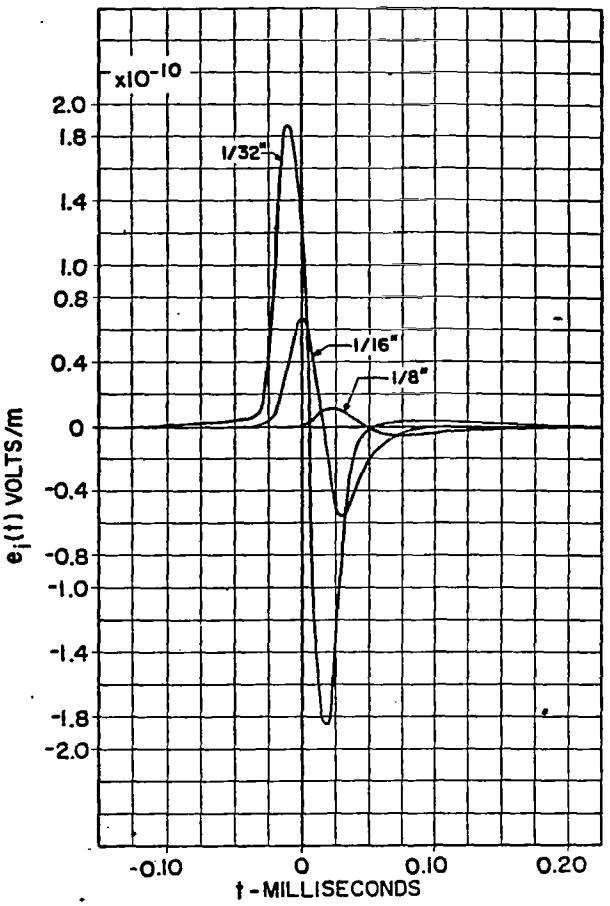

Graph 28—Cylinder. $e_o(o)=1$ vpm; $t_1=12$ μsec.

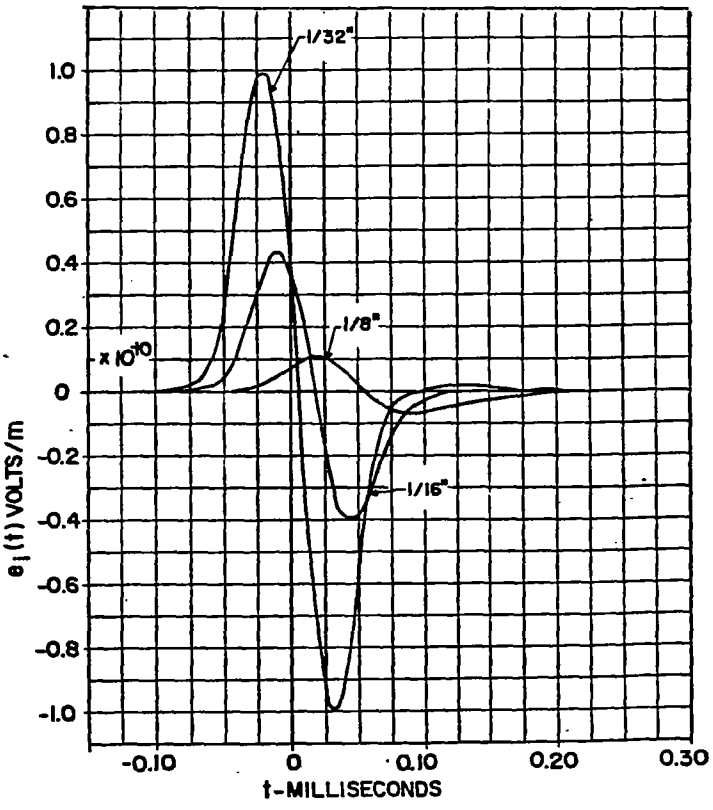

Graph 29—Cylinder. $e_o(o)=1$ vpm; $t_1=24$ μsec.

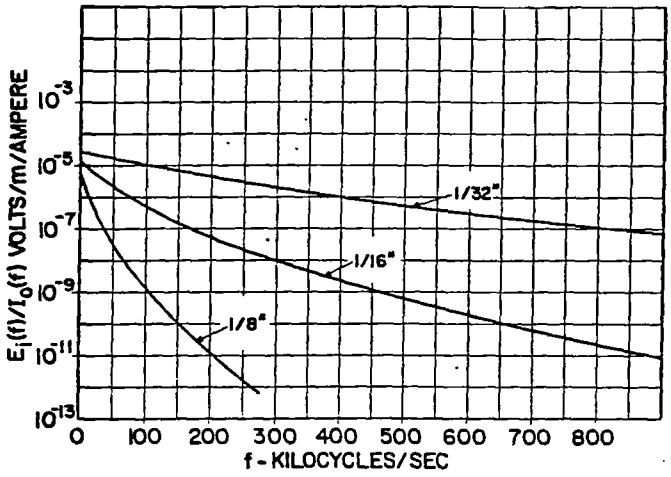

Graph 30—Cylinder. Steady-state transfer characteristic relating $E_i(f)$ to $I_o(f)$.

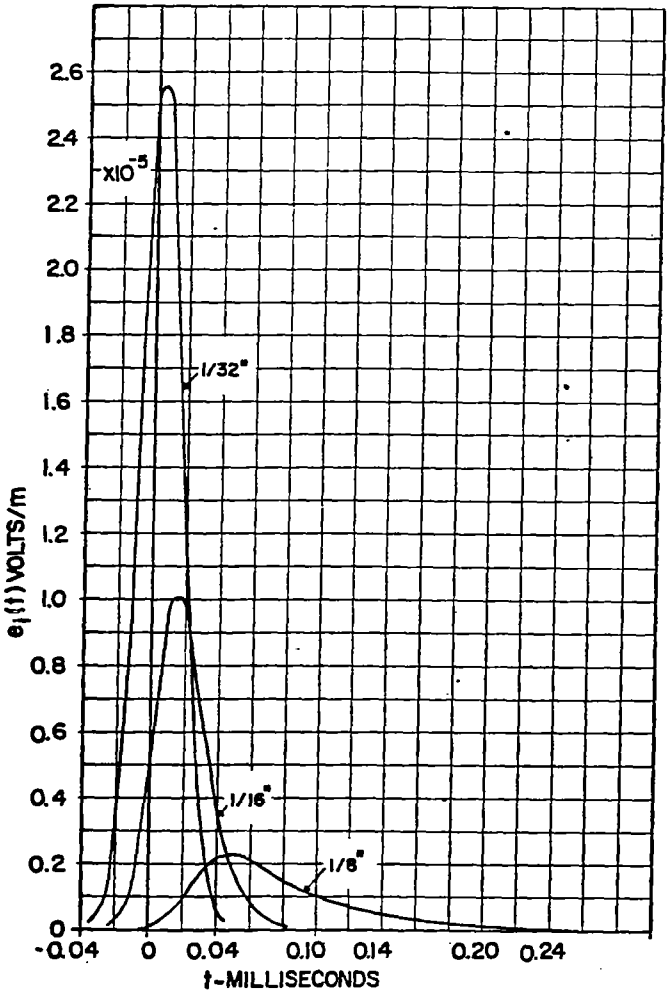

Graph 31—Cylinder. $i_o(o) = 1$ ampere; $t_1 = 12$ μsec.

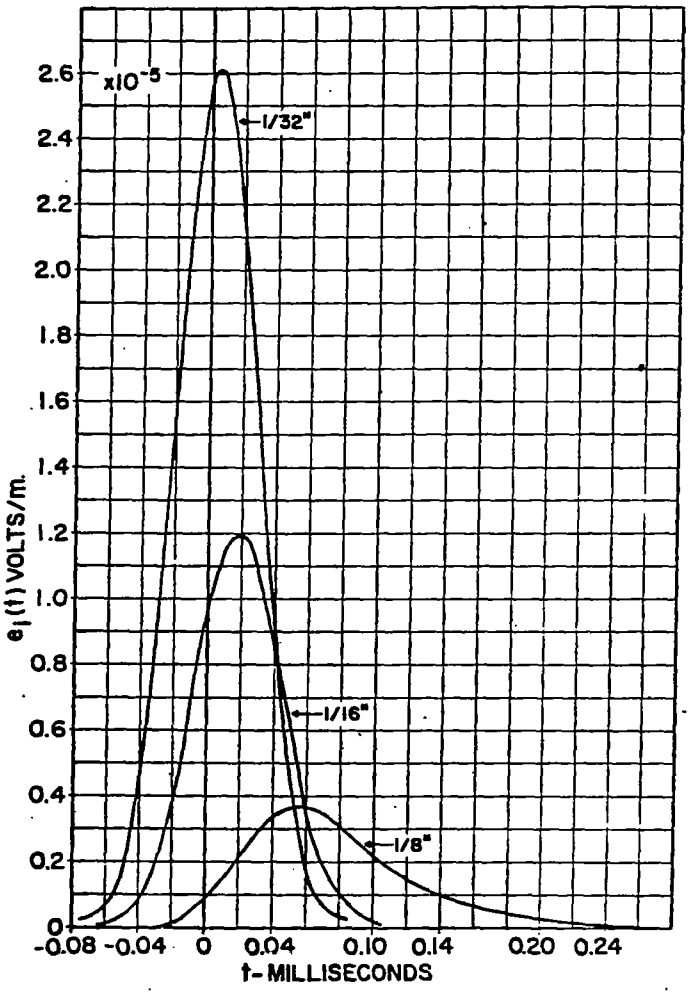

Graph 32—Cylinder. $i_o(o) = 1$ ampere; $t_1 = 24$ μsec.

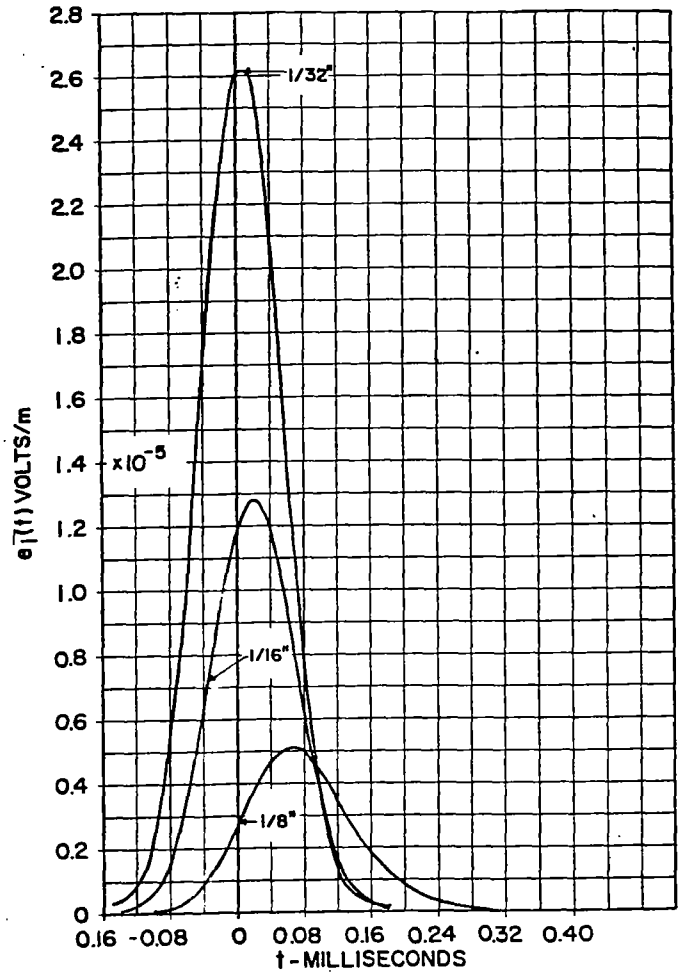

Graph 33—Cylinder. $i_s(o)=1$ ampere; $t_1=48$ μsec.

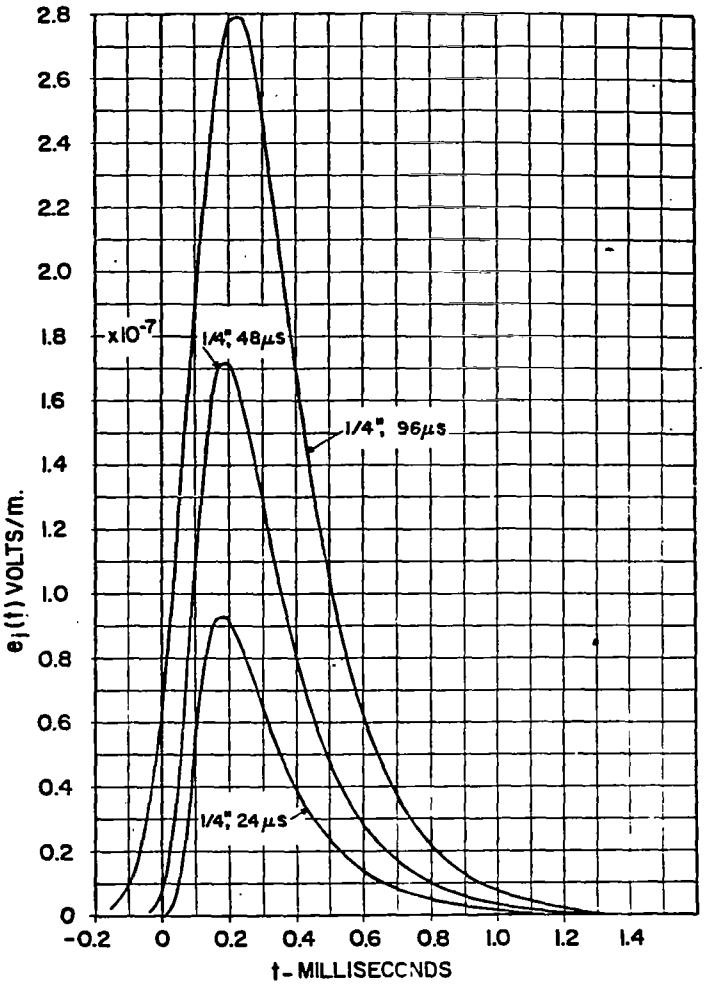

Graph 35—Jupiter missile. $i_s(o)=1$ ampere; $t_1=24$, 48, and 96 μsec.

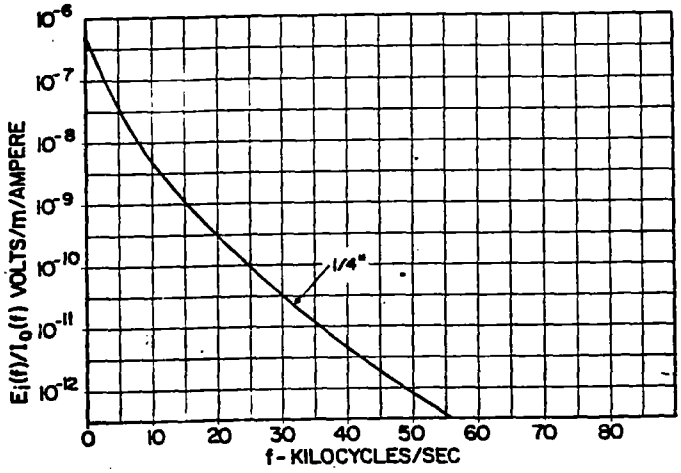

Graph 34—Jupiter missile. Steady-state transfer characteristic relating $E_i(f)$ to $I_s(f)$.

TABLE I

DECIBEL RATIO OF ENERGY AVAILABLE IN THE EMERGING PLANE-WAVE PULSE FROM THE FAR SIDE OF A PLATE TO THE ENERGY IN THE IMPINGING PLANE-WAVE PULSE ON THE NEAR SIDE OF THE PLATE

Case of the Tangential Electric Field			Case of the Incident Electric Field		
d	t_1	db	d	t_1	db
1/32 inch	6 μsec	− 3	1/32 inch	6 μsec	−135
1/16 inch	6 μsec	− 7	1/16 inch	6 μsec	−144
1/8 inch	6 μsec	−13	1/8 inch	6 μsec	−155
1/32 inch	12 μsec	− 1	1/32 inch	12 μsec	−135
1/16 inch	12 μsec	− 5	1/16 inch	12 μsec	−142
1/8 inch	12 μsec	−10	1/8 inch	12 μsec	−152
1/32 inch	24 μsec	0.0	1/32 inch	24 μsec	−135
1/16 inch	24 μsec	− 3	1/16 inch	24 μsec	−141
1/8 inch	24 μsec	− 7	1/8 inch	24 μsec	−150
1/32 inch	48 μsec	0.0	1/32 inch	48 μsec	−135
1/16 inch	48 μsec	− 1	1/16 inch	48 μsec	−141
1/8 inch	48 μsec	− 5	1/8 inch	48 μsec	−148

Concluding Remarks

The shielding action of aluminum plates, spherical shells and hollow cylinders to transient impinging fields and currents has been investigated rigorously. It has been assumed that the forcing pulses contain no frequencies sufficiently high to excite resonances in the spherical shells or hollow cylinders. The lowest mode of a perfectly conducting spherical shell is $\lambda_o = 2.28b$, where b is the inner radius. The lowest radial mode for a perfectly conducting cylinder when the exciting electric field is parallel to the axis of the cylinder is $\lambda_o = 2.61b$, where, again, b is the inner radius. The lowest longitudinal mode for the cylinder occurs when $2h \approx \lambda/2$. A moment's investigation will reveal that all of the cavity shields studied in this paper have dimensions sufficiently small that no resonances can be excited by a frequency $f_c = 68.96$ kc, which corresponds to $t_1 = 6\mu$sec. This is the smallest value of t_1 of any Gaussian pulse considered in the present analysis.

It should be evident to the reader that the use of Gaussian pulses is not dictated by any theoretical considerations. Suppose $e_o(t)$ corresponding to a lightning flash is measured. Then $E_o(f)$, the forcing function, can be found by numerical integration by using a truncated form of the Fourier integral

$$E_o(f) = \int_{-\infty}^{\infty} e_o(t) e^{-j2\pi ft} dt,$$

for passing from the time to the frequency domain.

Having found the frequency spectrum $E_o(f)$ corresponding to the time function $e_o(t)$, one can find $e_i(t)$ numerically by using a truncated form of the Fourier integral

$$e_i(t) = \int_{-\infty}^{\infty} G(f) E_o(f) e^{j2\pi ft} df.$$

Thus, $e_i(t)$ can be found for any arbitrary wave shape $e_o(t)$, just as easily as was done for Gaussian impinging pulses used in this paper.

In several instances in this paper, the magnitude of the steady-state transfer function continues to rise with increasing frequency beyond $f_c = 2.6f_1 = 2.6/2\pi t_1$. The results obtained for these cases were checked by extending the limit f_c of integration on (34) to higher frequencies. There were no significant changes in the numbers obtained.

Center-loaded electric dipoles may be placed axially in the cylinders, and impedance-loaded loops in the spherical shells and the energy in the loads evaluated under transient conditions. Consideration of these interesting problems is reserved for another paper.

Appendix I

The Necessity for Knowing the Time Dependence Employed in Deriving the Transfer Functions

It has been stressed that the time dependence employed in deriving the transfer functions given in this paper for sheets, spheres and cylinders is exp $(j2\pi ft)$. If the time dependence exp $(-j2\pi ft)$ (favored by many Electrodynamists) has been assumed in the development of (15), for example, the effect would have been to substitute k for γ. The transfer function then becomes $G^*(f)$ instead of $G(f) = H_i(f)/H_o(f)$. To obtain meaningful results in the solution of transient problems, this change must be reflected by appropriate sign changes in the exponents of the Fourier transforms for passing from the frequency to the time domain, and vice versa.

Consider a series RL circuit (assumed to be linear). The driving voltage is $e(t)$ and the current in the circuit is $i(t)$. The differential equation is

$$e(t) = L\frac{di(t)}{dt} + Ri(t).$$

Let $e(t) = e^{j2\pi ft}$. Then, $i(t) = G(f)e^{j2\pi ft}$ where $G(f) = 1/(R + j\omega L)$. (See Table II.) Since

$$e(t) = \int_{-\infty}^{\infty} E(f) e^{j2\pi ft} df,$$

for consistency,

$$E(f) = \int_{-\infty}^{\infty} e(t) e^{-j2\pi ft} dt.$$

Alternatively, if $e(t) = e^{-j2\pi ft}$, it follows that $G(f) = 1/(R - j\omega L)$,

$$i(t) = \int_{-\infty}^{\infty} E(f)G(f)e^{-j2\pi ft} df; \qquad e(t) = \int_{-\infty}^{\infty} E(f) e^{-j2\pi ft} df,$$

and

$$E(f) = \int_{-\infty}^{\infty} e(t) e^{j2\pi ft} dt.$$

TABLE II

Input	Output
$e(t)$	$i(t)$
$e^{j2\pi ft}$	$G(f)e^{j2\pi ft}$
$E(f)e^{j2\pi ft}df$	$E(f)G(f)e^{j2\pi ft}df$
$\int_{-\infty}^{\infty} E(f)e^{j2\pi ft}df$	$\int_{-\infty}^{\infty} E(f)G(f)e^{j2\pi ft}df$

Appendix II

Notes on the Machine Evaluation of the Cylinder Transfer Function[10]

Let

$$G(z_1, z_2) = \frac{J_o(z_1)N_1(z_1) - N_o(z_1)J_1(z_1)}{J_o(z_2)N_1(z_1) - N_o(z_2)J_1(z_1)} = \frac{M}{D},$$

where $z_i = z_{iR} - jz_{iI}$, $z_{iR} = z_{iI}$, $i = 1, 2$. Also, define $z_2 = z_1 + \delta$ (δ small).

A) As mentioned in the body of the paper, as $f \to o$, $G(o, o) = 1 + jo$.

B) When $o < R_e(z_1) \leq 5$, $G(z_1, z_2)$ may be evaluated directly using single-precision arithmetic (36 bits); however when $5 < R_e(z_1)$, $G(z_1, z_2)$ cannot be accurately evaluated directly using single-precision arithmetic because of loss of significant digits in the subtractions. In lieu of the extreme difficulties encountered in evaluating $G(z_1, z_2)$ with multiple-precision arithmetic, the following approximation was used.

Let

$$G(z_1, z_2) = \frac{M}{D} = \frac{M}{M + D - M},$$

where

$$D - M = N_1(z_1)\{J_o(z_2) - J_o(z_1)\} - J_1(z_1)\{N_o(z_2) - N_o(z_1)\}.$$

It is now possible to expand $J_o(z)$ and $N_o(z)$ in a Taylor series about z_1. Recalling that $z_2 = z_1 + \delta$,

$$J_o(z_1 + \delta) - J_o(z_1) = \delta J_o'(z_1) + \frac{\delta^2}{2!} J_o''(z_1) + \frac{\delta^3}{3!} J_o'''(z_1) + \cdots.$$

A similar expansion holds for $N_o(z_1+\delta) - N_o(z_1)$. Combining powers of δ, and realizing that all Bessel functions now have z_1 for their argument, yields

$$D - M = \delta\{N_1 J_o' - J_1 N_o'\} + \frac{\delta^2}{2!}\{N_1 J_o'' - J_1 N_o''\} + \cdots = \sum_{n=1}^{\infty} \frac{C_n \delta^n}{n!}$$

where $C_n = N_1 J_o^{(n)} - J_1 N_o^{(n)}$. It remains to evaluate C_n.

By virtue of the relationships $J_o' = -J_1$ and $N_o' = -N_1$, it follows that $C_1 = 0$. Since J_o and N_o satisfy Bessel's equation,

$$J_o''(z) = -\frac{J_o'(z)}{z} - J_o(z),$$

and

$$N_o'' = -\frac{N_o'(z)}{z} - N_o(z),$$

$$C_2 = N_1\left\{-\frac{J_o'}{z} - J_o\right\} - J_1\left\{-\frac{N_o'}{z} - N_o\right\} = -N_1 J_o + J_1 N_o = -M.$$

Differentiating $J_o''(z)$ and $N_o''(z)$ yields

$$J_o'''(z) = -\frac{J_o''(z)}{z} + \frac{J_o'(z)}{z^2} - J_o'(z),$$

$$N_o'''(z) = -\frac{N_o''(z)}{z} + \frac{N'(z)}{z^2} - N_o'(z).$$

As before, the terms involving J_o' and N_o' cancel and

$$C_3 = \frac{M}{z}\bigg|_{z=z_1} = \frac{M}{z_1}.$$

Differentiating again yields

$$J_o'''' = -\frac{J_o'''}{z} + 2\frac{J_o''}{z^2} - 2\frac{J_o'}{z^3} - J_o''.$$

A similar expression holds for N_o''''. Now

$$C_4 = C_2\left[\frac{2}{z_1^2} - 1\right] - \frac{C_3}{z_1} = -M\left[\frac{2}{z_1^2} - 1\right] - \frac{M}{z_1^2} = M\left[1 - \frac{3}{z_1^2}\right].$$

It was decided that four terms of the expansion would be satisfactory for better than 1 per cent accuracy in the range

$$5 < R_e(z_1) \leq 20.$$

One may now write

$$G(z_1, z_2) = \frac{M}{M + D - M} \simeq \frac{M}{M - \frac{\delta^2}{2!}M + \frac{\delta^3}{3!z_1}M + \frac{\delta^4}{4!}\left[1 - \frac{3}{z_1^2}\right]M} = \frac{1}{1 - \frac{\delta^2}{2!} + \frac{\delta^3}{3!z_1} + \frac{\delta^4}{4!}\left[1 - \frac{3}{z_1^2}\right]}.$$

This approximation was used for $5 < R_e(z_1) \leq 20$.

[10] Contributed by E. A. Aronson.

C) For $R_e(z_1) > 20$, two terms of the asymptotic expansion may be used. We have

$$M \equiv -\frac{2}{\pi z_1}$$

$$D \cong -\frac{2}{\pi\sqrt{z_1 z_2}}\left\{\cos\delta\left[1-\frac{3}{64 z_1 z_2}\right] + \frac{\sin\delta}{8}\left[\frac{1}{z_2}+\frac{3}{z_1}\right]\right\},$$

yielding

$$G(z_1, z_2) \simeq \sqrt{\frac{z_2}{z_1}}\left\{\frac{1}{\left[1-\frac{3}{64 z_1 z_2}\right]\cos\delta + \frac{1}{8}\left[\frac{1}{z_2}+\frac{3}{z_1}\right]\sin\delta}\right\}.$$

Acknowledgment

The author wishes to thank C. S. Williams, Jr., for his many contributions to this work. The problems discussed in the paper were programmed twice for the Sandia Laboratory CDC-1604 computer by E. A. Aronson. Different procedures were used each time to insure accuracy in the numerical work. The article was reviewed by Prof. Ronold W. P. King and Dr. Hans Schmitt, both of whom made useful suggestions for improvement. Mrs. Margaret Houston plotted the graphs which were inked under the direction of C. A. Tucker. The manuscript was typed by Mrs. Deyoe Stark.

References

[1] W. L. Anderson and R. K. Moore, "Frequency spectra of transient electromagnetic pulses in a conducting medium," IRE Trans. on Antennas and Propagation, vol. AP-8, pp. 603–607; November, 1960.
[2] P. I. Richards, "Transients in conducting media," IRE Trans. on Antennas and Propagation, vol. AP-6, pp. 178–182; April, 1958.
[3] J. R. Wait, "Shielding of a transient electromagnetic dipole field by a conductive sheet," *Canad. J. Phys.*, vol. 34, pp. 890–893; 1956.
[4] J. R. Wait, "Induction in a conducting sheet by a small current current carrying loop," *Appl. Sci. Res.* vol. B-3, p. 230; 1953.
[5] S. H. Zisk, "Electromagnetic transients in conducting media," IRE Trans. on Antennas and Propagation, vol. AP-8, pp. 229–230; March, 1960.
[6] N. R. Zitron, "Shielding of transient electromagnetic signals by a thin conducting sheet," *J. Res. NBS-D. Radio Propagation*, vol. 64D, no. 5, pp. 563–567; September–October, 1960.